

UC Davis

UC Davis Previously Published Works

Title

Climatic controls on soil clay mineral distributions in humid volcanic regions of Sumatra and Java, Indonesia

Permalink

<https://escholarship.org/uc/item/5266c9pj>

Authors

Lyu, Han
Watanabe, Tetsuhiro
Ota, Yoriko
et al.

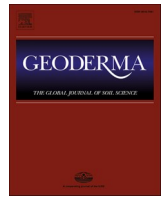
Publication Date

2022-11-01

DOI

10.1016/j.geoderma.2022.116058

Peer reviewed



Climatic controls on soil clay mineral distributions in humid volcanic regions of Sumatra and Java, Indonesia

Han Lyu^a, Tetsuhiro Watanabe^{a,b,*}, Yoriko Ota^b, Arief Hartono^c, Markus Anda^d, Randy A. Dahlgren^e, Shinya Funakawa^{a,b}

^a Graduate School of Global Environmental Sciences, Kyoto University, Kyoto 606-8501, Japan

^b Graduate School of Agriculture, Kyoto University, Kyoto 606-8502, Japan

^c Faculty of Agriculture, IPB University, Bogor 16680, Indonesia

^d Indonesian Center for Agricultural Land Resources Research and Development, Bogor 16114, Indonesia

^e Department of Land, Air and Water Resources, University of California Davis, Davis 95616, CA, USA

ARTICLE INFO

Handling Editor: Budiman Minasny

Keywords:

Mineral stability
Allophane
Gibbsite
Kaolinite
Andisol/Andosol
Silicic acid activity

ABSTRACT

Climate and parent material are considered the primary factors determining the distributions of soil clay (secondary) minerals, but their influence has not been rigorously elucidated for tropical volcanic soils. Herein, we investigated soil secondary mineral distributions in volcanic regions of Java and Sumatra islands representing large variations in climatic (mean annual temperature (MAT): 13 to 27°C; precipitation: 1910 to 3950 mm) and parent material conditions (rhyolitic-to-basaltic tephra). Soil secondary minerals were assessed by selective extractions, X-ray diffraction analysis, and differential thermal analysis. Moreover, the thermodynamic stabilities of minerals were evaluated based on the ion activities of equilibrated soil–water suspensions. Factor analysis of climate and soil geochemical (e.g., total Si, Fe and K) properties identified temperature, dry season intensity, and parent material as the primary factors regulating secondary mineral distributions. A negative correlation between oxalate extractable Al and Fe (Al_o and Fe_o) and the temperature factor indicates low temperature promoted the formation and preservation of short-range-order (SRO) minerals and organo-Al/Fe complexes, which resulted in $Al_o + 1/2Fe_o \geq 20 \text{ g kg}^{-1}$ (andic property criterion) at $MAT < 21^\circ\text{C}$. Desiccation in the dry season, represented by excess precipitation for the driest quarter of the year, was related to soil $H_4SiO_4^0$ activity of soil–water suspensions. High $H_4SiO_4^0$ activity resulting from intense seasonal desiccation coincided with a higher Si/Al ratio of SRO aluminosilicates (Si-rich allophane) and smectite. In contrast, low $H_4SiO_4^0$ activity enhanced the formation of SRO aluminosilicates with a low Si/Al ratio (Al-rich allophane) and gibbsite. The influence of parent materials was evident in high free Fe(hydr) oxide content in soils derived from mafic materials and the occurrence of mica, which altered to hydroxy-Al interlayered vermiculite under continuous leaching conditions, in soils from felsic materials. Overall, we demonstrated strong temperature and seasonal desiccation controls on secondary mineral distributions in the humid, tropical volcanic soils of Java and Sumatra islands.

1. Introduction

Clay (or secondary) minerals play an essential role in controlling soil physicochemical properties, including cation exchange capacity (CEC)/sorption dynamics, carbon stabilization, water holding capacity, and shrink/swell characteristics. For example, 2:1 clay minerals, such as smectite and vermiculite, strongly contribute to soil CEC via their high constant charge density (70–90 and 100–150 $\text{cmol}_c \text{ kg}^{-1}$, respectively) (Buol et al., 2011; Sharma et al., 2015). Further, active (i.e., oxalate-

extractable) Al and Fe have a strong ability to stabilize organic matter through organo-mineral interactions, thereby affecting both the quantity and quality of soil organic carbon, especially in volcanic soils (Asano and Wagai, 2014; Huang et al., 2016; Lyu et al., 2021; Takahashi and Dahlgren, 2016). Hence, understanding factors controlling the distribution of active Al and Fe, especially in tropical regions that experience rapid carbon cycling, is important for anticipating the response of these soils to climate change and land management activities. Additionally, active Al and Fe constituents disproportionately contribute to the

* Corresponding author at: Graduate School of Agriculture, Kyoto University, Kyoto 606-8502, Japan.

E-mail address: watanabe.tetsuhiro.2m@kyoto-u.ac.jp (T. Watanabe).

<https://doi.org/10.1016/j.geoderma.2022.116058>

Received 22 April 2022; Received in revised form 12 July 2022; Accepted 13 July 2022

Available online 25 July 2022

0016-7061/© 2022 Elsevier B.V. All rights reserved.

adsorption of phosphate and depress the plant availability of phosphate (Huang et al., 2002; Watanabe et al., 2015). Thus, understanding the distribution of soil secondary minerals and the factors controlling their distribution are fundamental and essential knowledge for agricultural and environmental management.

Understanding the formation of secondary soil minerals can be facilitated by studying their distributions with respect to climate and parent materials, the primary factors regulating the clay mineralogy of soils. Soils that develop from volcanic materials generally contain both short-range-order (SRO) minerals (e.g., allophane, imogolite, ferrihydrite) and crystalline clay minerals, which dominantly reflect the role of temperature and moisture conditions dictating the nature and intensity of the weathering/leaching regime (Churchman and Lowe, 2012; Lyu et al., 2018). For example, low temperature retards the crystallization process and promotes the preferential formation of SRO minerals incorporating Al, Fe, and Si (Churchman and Lowe, 2012; Lyu et al., 2018). The content of SRO minerals increases with temperature from cryic to mesic systems because the release of Al and Si from primary minerals is limited under freezing conditions (cryic), and the formation of SRO aluminosilicates is inhibited (Rasmussen et al., 2007). The high temperature and precipitation in tropical regions can promote the formation of crystalline clay minerals, such as gibbsite, kaolins, and 2:1 type minerals (Churchman and Lowe, 2012; Lyu et al., 2018; Van Ranst et al., 2020).

Coupled with temperature, soil moisture strongly influences the neoformation of SRO and crystalline minerals. High precipitation and low evapotranspiration were shown to create an intensive leaching regime, thereby favoring neoformation of SRO aluminosilicates in volcanic materials within a subtropical monsoon climate (Tsai et al., 2010). Similarly, $H_4SiO_4^0$ activity and pH of soil solutions are strongly linked to precipitation/leaching, thereby affecting the abundance and composition of aluminosilicates (Al-rich vs Si-rich allophane, halloysite vs kaolinite, kaolins vs smectite) (Dahlgren et al., 2004; Takahashi et al., 1993). Gibbsite, kaolin minerals, and smectite are formed through neoformation and are differentiated primarily by differences in ion activities (e.g., $H_4SiO_4^0$, Al^{3+} , Mg^{2+}) and pH of the soil solution (Karthanas, 2002; Watanabe et al., 2006). Gibbsite is generally abundant in soils with high leaching intensity and low $H_4SiO_4^0$ activity in subhumid volcanic and humid non-volcanic tropical climates (Lyu et al., 2018; Watanabe et al., 2017). The intensity of soil dry-wet alternation cycles may further regulate the formation of kaolin minerals and smectite in arid to semiarid soils (Churchman and Lowe, 2012; Churchman et al., 2016; Rasmussen et al., 2010; Ziegler et al., 2003).

In addition to climate, the Si and base cation content of parent materials affect aqueous pH and $H_4SiO_4^0$ activities (Harsh et al., 2002) and the weatherability of the parent material (Rasmussen et al., 2010; Rasmussen et al., 2007; Vingiani et al., 2004). For example, the formation of smectite and kaolin minerals appears to be favored in soils derived from basaltic (mafic) versus rhyolitic (felsic) materials (Rasmussen et al., 2010; Vingiani et al., 2004). Additionally, the formation of vermiculite is associated with mica alteration, which is promoted under intensive leaching conditions when mica is present in parent material (e.g., felsic rocks) (Watanabe et al., 2006). Despite the numerous soil clay mineralogy studies examining the effects of climate and parent materials on the distribution of SRO and crystalline minerals, there is a distinct paucity of studies addressing humid tropical volcanic soils.

Indonesia has a series of volcanic soils distributed across Sumatra and Java islands, providing an ideal setting for examining the effects of climate and parent material on the distribution of soil secondary minerals under humid tropical conditions. The climate in the volcanic regions of Indonesia is sharply contrasting with previous studies examining climate effects on the clay mineralogy of volcanic soils, such as the Mediterranean climate in western North America and southern Europe (Rasmussen et al., 2010; Vingiani et al., 2004), the temperate oceanic climate of Oceania (Cunningham et al., 2016; Singh et al., 2017), and the temperate monsoon climate of eastern Asia (Shoji and

Takahashi, 2002; Takahashi and Shoji, 1996). The temperature and moisture changes that occur along elevational gradients in the volcanic regions of Indonesia provide a wide range of chemical weathering regimes to assess how climate influences the distribution of secondary minerals. In addition, the parent materials for volcanic soils in Indonesia span mineralogical compositions from basaltic to rhyolitic tephra deposited by Quaternary volcanic eruptions (Amin et al., 1999; Gafoer et al., 1996; Gafoer et al., 2012; Gafoer and Ratman, 1999; Ratman and Gafoer, 1998; Siebert et al., 2011). While the distribution and properties of soil secondary minerals in Indonesia have been previously reported (e.g., Anda and Dahlgren, 2020; Van Ranst et al., 2008; Van Ranst et al., 2002), few studies have investigated soils across the broader range of climatic (temperature and precipitation, along a wide elevation gradient) and parent material conditions of both Sumatra and Java islands.

The objective of this study was to assess the effects of climate and parent material on the distribution of soil secondary minerals in the tropical volcanic regions of Indonesia. A total of 42 sites spanning large temperature (13.0–26.6°C) and precipitation (1910–3950 mm) gradients, as well as contrasting parent materials, were investigated across Sumatra and Java islands. The total elemental composition was used to assess parent material and soil weathering degree. The stabilities of secondary clay minerals were assessed using equilibrated soil–water suspensions to investigate the chemical conditions favoring the formation of specific SRO and crystalline clay minerals. We expected the contrasting pedogenic conditions associated with the wide range of climate and parent materials to help us elucidate the primary factors regulating the formation of SRO and crystalline clay minerals in tropical volcanic soils.

2. Materials and methods

2.1. Study area and soil sampling

Sampling sites ($n = 42$ sites) were selected across the volcanic regions of Sumatra and Java islands, Indonesia (Fig. 1) and designated as North Sumatra (NS, $n = 9$), Central–South Sumatra (SS, $n = 11$), West Java (WJ, $n = 4$) and Central–East Java (EJ, $n = 18$). Sites were selected along an elevation gradient ranging from 80 to 2260 m asl (Tables 1 and S1). Climate data were obtained from the WorldClim database, including monthly and annual temperature and precipitation data (representative of 1970–2000, 174 climatic stations for Java and 348 climatic stations for Sumatra and with additional satellite data, of which coordinates can be obtained from databasin.org; Fick and Hijmans, 2017) (Table 1). Mean annual air temperatures ranged from 13.0 to 26.6°C and mean annual precipitation from 1910 to 3950 mm, which resulted in soil temperature regimes of isothermic to isohyperthermic, and soil moisture regimes of ustic to perudic (Soil Survey Staff, 2014) (Tables 1 and S1). Potential evapotranspiration for each site was estimated based on monthly temperatures (Thornthwaite, 1948). Excess precipitation (EP) was calculated as precipitation minus potential evapotranspiration (Tables 1 and S1) and used as an indicator of leaching intensity. Excess precipitation for the driest quarter of the year (EPDQ) was calculated and used as a metric of desiccation intensity during the dry season (Tables 1 and S1).

Geological information for the study sites was obtained from geological maps of Indonesia (Amin et al., 1999; Crow and Barber, 2005; Gafoer et al., 1996; Gafoer et al., 2012; Gafoer and Ratman, 1999; Ratman and Gafoer, 1998) (Tables 1 and S1). All soils formed on tephra deposits from Quaternary volcanic activity probably occurring during the late-Pleistocene or later, considering the activity of volcanoes throughout the region (Global-Volcanism-Program, 2013). To specify the exact age of parent materials was difficult because of the high activity and close distribution of volcanoes. Our best estimates of the major volcanic source and eruption time are given in Table S1. The geologic composition of tephra deposits for North Sumatra was

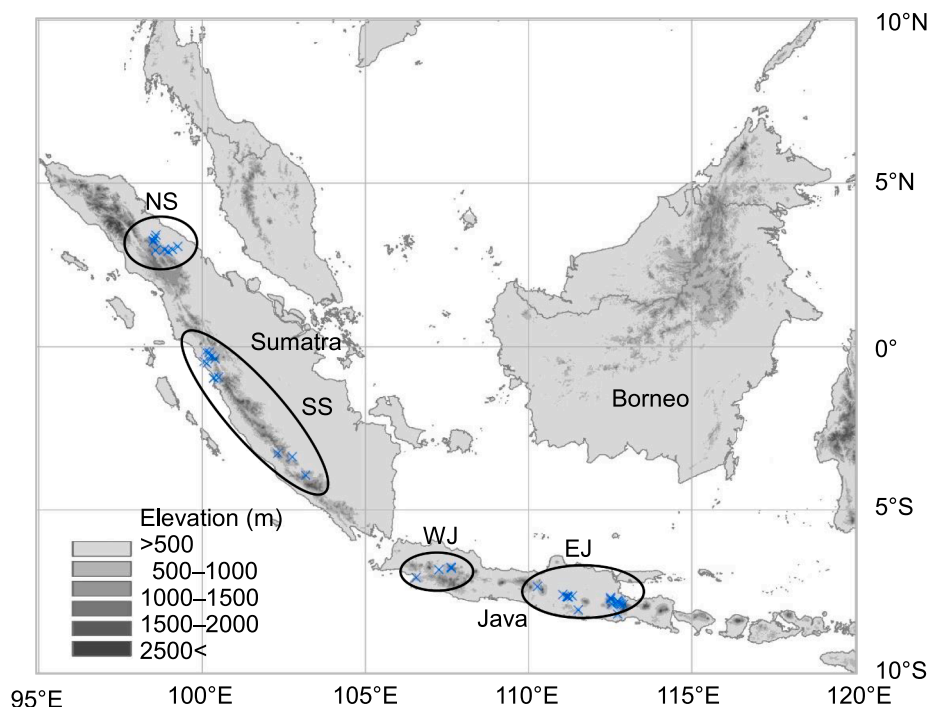


Fig. 1. Locations of soil sampling (crosses) in four regions (North Sumatra (NS): 9 sites, Central and South Sumatra (SS): 11 sites, West Java (WJ): 4 sites, Central and East Java (EJ): 18 sites) of Indonesia.

Table 1
Fundamental information of studied regions.

Region	Sites No.	Parent materials ^a	Elevation m	MAT ^b °C	MAP ^b mm	EP ^b mm	EPDQ ^b mm	Soil classification ^c	pH	TC g kg ⁻¹	NPP ^d g C m ⁻² yr ⁻¹
North Sumatra (NS)	9	Rhyolitic, Andesitic to dacitic tephra	110–1520	18.7–26.2	2190–2950	960–1750	19–270	Udands (4), Udepts (4), Udults (1)	4.4–5.4	2.8–110	940–1020
Central and South Sumatra (SS)	11	Rhyolitic, Andesitic to dacitic tephra (6); Andesitic–basaltic tephra (5)	80–1420	19.0–26.6	2160–3730	1310–2120	48–330	Vitrands (1), Udands (4), Udepts (3), Udults (3),	4.4–5.6	6.6–48	940–1030
West Java (WJ)	4	Andesitic–basaltic tephra	300–1500	18.2–25.4	2380–3950	950–2770	–52–190	Udands (2), Udepts (1), Uderts (1)	4.7–6.5	4.6–77	970–1030
Central and Eastern Java (EJ)	18	Andesitic–basaltic tephra	290–2260	13.0–25.3	1910–3300	570–2390	–130–61	Vitrands (2), Ustands (5), Udands (3), Ustepts (2), Udepts (1), Ustalfs (5)	4.6–6.8	4.2–56	800–1030

^a Geological information for the study sites was obtained from Geological Maps of Indonesia (Amin et al., 1999; Crow and Barber, 2005; Gafoer et al., 1996; Gafoer et al., 2012; Gafoer and Ratman, 1999; Ratman and Gafoer, 1998).

^b MAT, mean annual temperature; MAP, mean annual precipitation; EP, excess precipitation; EPDQ, excess precipitation for the driest quarter.

^c Soil classification is according to the Keys to Soil Taxonomy (Soil Survey Staff, 2014).

^d NPP, potential net primary production.

rhyodacitic-to-andesitic, whereas Central–South Sumatra sites were rhyolitic, dacitic-to-andesitic, and andesitic-basaltic (Crow and Barber, 2005; Gafoer et al., 1996; Gafoer et al., 2012). The parent materials for Java sites were andesitic-basaltic (Amin et al., 1999; Gafoer and Ratman, 1999; Ratman and Gafoer, 1998).

Soil sampling locations were mostly located under tree vegetation (secondary forest or tree plantations, such as teak, pine, and cacao) with several exceptions (6 grassland sites and 2 fallowed agricultural fields) at ridge, gentle shoulder slope, or foothill positions (0–5 % slope). Potential net primary production was estimated using the mean average temperature (MAT) and precipitation (MAP) values (Del Grosso et al.,

2008). All soils were well-drained, and there was no evidence of accelerated erosion. A soil pedon was excavated to a depth of ~80 cm at each site (Fig. S1), and soil horizons and morphological properties were described in the field. Soil samples were collected from three sides of each pedon, and a well-mixed composite sample was acquired for each horizon (Pennock et al., 2007). Samples were air-dried, gently crushed, sieved (2-mm), and mixed again before laboratory analyses. We specifically focused on the characterization of the physical, chemical, and mineralogical properties of B horizon soils collected from about 30 to 60 cm depth to minimize potential discrepancies associated with recent volcanic and human activities. According to the global soil regions map

(https://www.nrcs.usda.gov/wps/portal/nrcs/detail/soils/use/?cid=nrcs142p2_054013), field observation and physicochemical analyses, soils were classified as Andisols (21), Inceptisols (11), Ultisols (4), Alfisols (5), and Vertisols (1) based on USDA Soil Taxonomy (Soil Survey Staff, 2014).

2.2. Analytical methods

Total elemental analysis for air-dried soils (ground by ball mill) was determined by digestion in a sealed Teflon container with a mixture of HF and aqua regia (Hossner, 1996). The digested solution was filtered through a 0.45- μm membrane filter (Millipore) and quantified by inductively coupled plasma atomic emission spectrometry (ICP-AES; ICPE-9000, Shimadzu, Kyoto, Japan). The total reserve bases (TRB) weathering index was defined as the sum of total K, Na, Ca, and Mg contents ($\text{cmol}_c \text{kg}^{-1}$) (Lyu et al., 2018; Watanabe et al., 2017). All values are reported on an oven-dried soil basis (Delvaux et al., 1989; Hossner, 1996).

Soil pH was measured using a pH meter (F-70 Series, Horiba, Kyoto, Japan) at a 1:5 (g:mL) soil to solution (H_2O) ratio after equilibration for 1 h. Total C and N contents were measured by combustion using an elemental analyzer (Vario MAX, Elementar Analysensysteme, Hanau, Germany); no carbonate minerals were present in soils. Exchangeable Ca^{2+} and Mg^{2+} were extracted by 1 M NH_4OAc (pH 7.0) and determined by atomic absorption spectroscopy, whereas exchangeable K^+ and Na^+ were quantified by flame emission spectroscopy (AA-660, Shimadzu, Kyoto, Japan). Then soil CEC was determined based on adsorbed NH_4^+ after washing the extracted soil with 10 % NaCl. Before soil particle size analysis, organic matter was oxidized by boiling with 10 % H_2O_2 , pH adjusted to 9–10 or 5 when soil particles were not dispersed under alkaline conditions (pH 9–10), and ultrasonic dispersion for 15 min. The sand (0.02–2 mm) fractions were determined by sieving, whereas the silt (2–20 μm) and clay (<2 μm) fractions were determined using the pipette method (Stokes' law) (Gee and Or, 2002). Particle-size classes were according to the International Soil Science Society. Both the silt and clay fractions were collected for subsequent mineralogical analysis.

Ammonium oxalate (0.2 M, pH 3.0, 4 hr shaking, dark) was used to quantify active Al, Fe, and Si (Al_o , Fe_o , and Si_o) (Blakemore, 1987). Further, organo-metal complexes (Al_p and Fe_p) were extracted using Napyrophosphate (0.1 M, pH 10.0) by shaking for 16 h at 25°C (Blakemore, 1987). Free iron (hydr)oxides (Fe_d) were extracted with a mixture of citrate (0.75 M) and hydrosulfite sodium (dithionite; 1 g in 50 mL) (Blakemore, 1987). The ammonium oxalate and dithionite-citrate extracts were filtered through a 0.45- μm membrane filter (Millipore). Napyrophosphate extracts were filtered through a 0.025 μm membrane filter (Millipore). The contents of Al, Fe, and Si in the extracts were measured by ICP-AES. Because of a wide range of ($\text{Al}_o - \text{Al}_p$)/ Si_o ratios, the content of the allophanic materials was calculated using the formula $\text{Si}_o \times 1.36 ((\text{Al}_o - \text{Al}_p) / \text{Si}_o)^2 - 1.76 ((\text{Al}_o - \text{Al}_p) / \text{Si}_o) + 5.44$ based on the data of Parfitt (1990). The content of ferrihydrite was calculated by multiplying the Fe_o by 1.7 (Childs, 1985).

The crystalline mineral composition of the clay and silt fractions was determined using X-ray diffraction (XRD) (Miniflex 600, Rigaku, Tokyo, Japan) with $\text{Cu K}\alpha$ radiation (40 kV, 15 mA). The clay and silt fractions isolated following particle size analysis were air-dried, and parallel-oriented slides were treated as follows for XRD analyses: (1) Mg^{2+} saturated and dried at 25°C, (2) solvated in glycerol after Mg^{2+} saturation and dried at 25°C; and (3) K^+ saturated and heated at 25°C, 350°C and 550°C (Harris and White, 2008). A separate clay aliquot was treated with formamide to distinguish 0.7-nm halloysite (dehydrated halloysite that is expandable to 1.0 nm by formamide) from the 0.7-nm kaolinite peak using XRD (Churchman et al., 2010; Churchman et al., 1984). Before and after formamide treatment, change in peak height was examined to determine whether kaolinite or halloysite was dominant. XRD peaks for the Mg^{2+} saturated slide was classified into four semi-quantitative categories: clearly detected with a dominant peak (higher

than twice that of other peaks), clearly detected, not clearly detected (higher than twice but lower than five times the background noise), and not detected (Fig. S2). Differential thermal analysis (DTA) was applied to quantify gibbsite and kaolin contents in the clay fraction using a TA-60WS thermal analyzer equipped with a simultaneous DTA–thermogravimetric apparatus (DTG60, Shimadzu, Kyoto, Japan) (Fig. S3). We used Al hydroxides (Wako, Osaka, Japan) and Georgia kaolin (Nichika, Kyoto, Japan) as standards for gibbsite and kaolin, of which the calibration curves were confirmed by thermogravimetry. The DTA heating rate was 20°C min^{-1} in an N_2 atmosphere (Watanabe et al., 2017). Before DTA, free Fe (hydr)oxides were removed from clay fractions by dithionite-citrate solution (pH 7.3) in an 80°C water bath to avoid interferences from free Fe (hydr)oxides on gibbsite quantification.

The stabilities of secondary minerals were assessed based on the ion activities of soil–water suspension. A soil–water suspension of each soil sample was prepared by equilibrating 80 g soil in 160 mL deionized water for one week at 25°C and 101 kPa. The suspensions were shaken once a day (Watanabe et al., 2017). Then, the equilibrated solution was passed through a 0.025- μm membrane filter (mixed cellulose esters, Millipore). The filtrate pH and F^- were determined using ion-selective electrodes (pH/mV meter F-70 Series, Horiba, Kyoto, Japan). Concentrations of Al, Fe, and Si were measured by ICP-AES. The Al concentration was measured both before and after passing through a column of pH-adjusted (based on average pH of filtered solutions) cation exchange resin (Amberlite, IR-120B(H)). The Al retained by the resin was assumed to be inorganic monomeric Al ion species (Driscoll, 1984). Dissolved inorganic C (DIC-carbonates) was determined using a carbon analyzer (TOC-V CSH, Shimadzu, Kyoto, Japan). Concentrations of cations (Ca^{2+} , Mg^{2+} , K^+ , Na^+ , and NH_4^+) and anions (Cl^- , NO_3^- , and SO_4^{2-}) (Columns: Shim-pack IC-C3 for cations, Shim-pack ICC-A1 for anions) were determined using high-performance liquid chromatography (HPLC-HIC-6A equipped with a CDD-6A detector, Shimadzu, Kyoto, Japan).

Ion activities for each sample were calculated using Visual MINTEQ ver. 3.1 (Gustafsson, 2014). Solubility and stability diagrams for common clay minerals were constructed and compared to ion activities (Van Breemen and Brinkman, 1976). The thermodynamic equilibrium constants used in the solubility and stability diagrams for kaolinite, gibbsite, smectite, quartz, and amorphous SiO_2 were taken from Karathanasis (2002), muscovite from Lindsay (1979), halloysite and imogolite from Dahlgren and Ugolini (1989), and allophane from Sigfusson et al. (2008). The chemical reactions and equilibrium constants of the minerals are listed in Table S2. We expressed mineral stabilities in two ways: a solubility diagram (Karathanasis, 2002), which shows precipitation-dissolution equilibrium lines for minerals, and a stability diagram (Van Breemen and Brinkman, 1976), which shows relative stability fields for selected minerals. Though solubility diagrams theoretically include similar information as in stability diagrams, the stability diagrams do not require an Al^{3+} activity term, which is difficult to determine precisely in solutions with near-neutral pH values, and therefore are considered more reliable for assessing the relative stability of minerals.

2.3. Statistical analyses

Factor analysis was conducted based on the standardized (z-score) total elemental contents (Si, Al, Fe, Ca, Mg, K, Na, and Ti) to investigate the parent materials and weathering conditions for each sampling region. We applied factor analysis to simplify the variables believed to affect the distribution of SRO and crystalline clay minerals. Specifically, we assessed climate data (mean annual temperature and precipitation, excess precipitation, and excess precipitation during the driest quarter), total Si, Fe, and K contents (representing the nature of parent materials—felsic vs mafic), a weathering index (TRB), and selected soil properties (pH, H_4SiO_4^0 activity in soil–water suspension and total C). The Shapiro-Wilk test was used to confirm the normality of climatic data, the physicochemical and mineralogical properties of soils, and factor scores.

Spearman rank correlation was applied to assess relationships among the variables due to the low passing rate of normality tests even after transformations. The detection levels of crystalline minerals by XRD were ranked for correlation analysis as not detected (0), not clearly detected (1), clearly detected (2), and clearly detected with a dominant peak (3). One-way ANOVA and multiple comparisons with Tukey-Kramer (equal variances), Tamhane's T2, or Dunnett's T3 (unequal variances) post-hoc tests were used to determine statistical differences (two-tailed) in climatic properties, total elemental compositions, and soil physicochemical and mineralogical properties between regions. Statistical analyses were performed using IBM SPSS version 24.0, JMP 14, and R (ver. 4.1.1) at a $P < 0.05$ significance level unless otherwise mentioned.

3. Results

3.1. Climate and parent material

While the mean annual precipitation was high (>1900 mm) for all sites, the soil moisture regimes ranged from perudic and udic for Sumatra (NS and SS) and West Java (WJ) to udic and ustic for Central-East Java (EJ) (Tables 1 and S1). Mean annual temperature decreased linearly as elevation increased ($r_s = -0.99$, $P < 0.001$). Though potential evapotranspiration was lower at higher elevations with lower temperatures, the correlation between EP and elevation was weak ($r_s = 0.32$, $P < 0.05$), implying that EP mostly reflects regional differences. The EP in the driest quarter was significantly lower at EJ (-41 ± 86 mm) than in the other regions (Table S3).

Total elemental analysis was applied to investigate the parent material and weathering condition of soils (Table 2). Total Fe contents were significantly lower in NS soils (51 ± 27 g kg⁻¹) than EJ soils (83 ± 20 g kg⁻¹). Total Si and TRB were high for all sites, and the difference among regions was not significant (Table 2), suggesting limited desilication and high primary mineral contents. There was no significant difference in TRB between soils derived from felsic (NS and SS) versus mafic (WJ and EJ) tephra (Table 2). This implies that the TRB values are more related to the weathering degree than the original parent materials of the studied soils. Total Si content was negatively correlated with total Fe and positively correlated with total K and Na, whereas total Fe content was positively correlated with total Ti and negatively correlated with total K and Na (Table S4). These correlations reflect the contrasting elemental composition of felsic versus mafic rocks. The positive correlation between total Si and total K or Na (Table S4) indicates that Si was associated with base elements in primary minerals (e.g., alkaline feldspars and mica). There was no correlation between MAT and total Si or TRB (Fig. S4), thereby indicating no clear trend in desilication and primary mineral contents along the elevational gradients.

Factor analysis was applied further to investigate the total elemental results (Tables 2 and S5). The first component was the "Fe-Ti vs Si-K" factor (34 %), which primarily reflects the parent material composition (i.e., mafic versus felsic). The second component was the "Ca-Mg-Na" factor (27 %), which represents the remaining base elements and thereby an index of weathering. The diagram of scores showed that NS had low scores for the "Fe-Ti vs Si-K" factor, whereas EJ had a high score

for the "Fe-Ti vs Si-K" factor (Fig. 2). Differences in the "Ca-Mg-Na" factor scores, thus weathering degrees, were not evident between regions.

3.2. Soil physicochemical properties

The physicochemical properties of soils for each region are shown in Table 3 (more details in Table S6). Soil pH was acidic to near neutral (4.4 to 6.8) and significantly lower at NS and SS than EJ (Table 3). Other physicochemical properties were similar between regions (Table 3). A significant negative correlation ($r_s = -0.65$, $P < 0.001$) was found between EPDQ and soil pH but not between EP and pH (Fig. S4). H₄SiO₄ activity in the soil-water suspension also correlated with EPDQ, but not with EP (Fig. S4). Low clay contents (<20 %) were observed for 12 of 18 soils at high elevation sites (>1000 m asl). Clay contents were relatively higher at the low elevation sites having a higher MAT (Fig. S4). Conversely, total C and N contents increased with a decrease in MAT. Potential net primary production was similar for the different sites (Table 1), implying a negligible impact of C inputs on soil C contents.

3.3. Factor analysis of climatic and geochemical variables

Factor analysis of variables suspected to affect distributions of SRO and crystalline clay minerals yielded four factors, which explained 78 % of the total variation (Table 4). The first factor (22 % of explained

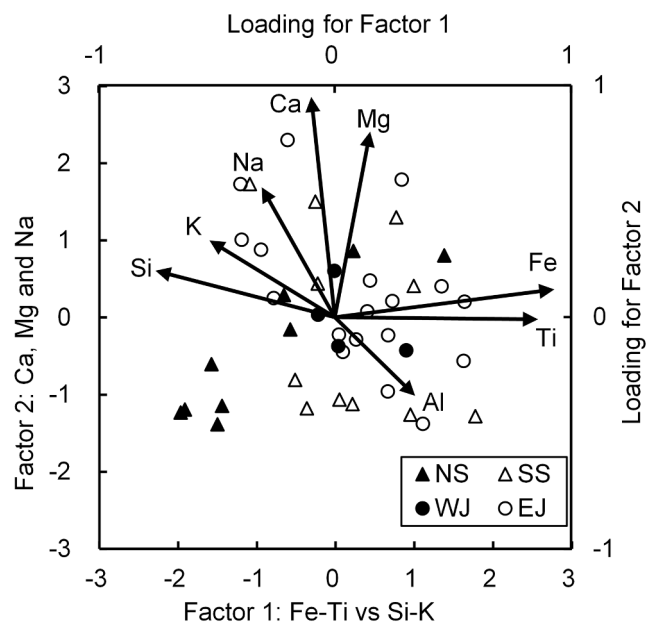


Fig. 2. Diagram of factor analysis for total elemental compositions of B horizon soils from four sampling regions (42 sites). (NS, North Sumatra; SS, Central and South Sumatra; WJ, West Java, EJ: Central and East Java).

Table 2

Total elemental contents of the oven-dry, fine-earth fraction of B horizon soils in studied regions.

Region ^a	Number of sites	Si	Al	Fe	Ti	Ca	Mg	K	Na	TRB ^b
		g kg ⁻¹								cmolc kg ⁻¹
NS	8	280 ± 38	130 ± 29	51 ± 27b	4.3 ± 2.1b	8.2 ± 6.3	6.9 ± 6.1	12 ± 4	11 ± 13	180 ± 94
SS	11	260 ± 55	130 ± 33	74 ± 14 ab	7.0 ± 1.2 a	10 ± 11	9.4 ± 8.2	6.3 ± 6.6	8.1 ± 10.9	180 ± 150
WJ	4	260 ± 54	100 ± 22	72 ± 15 ab	7.2 ± 2.5 a	12 ± 4.2	9.1 ± 5.9	4.3 ± 2.6	4.5 ± 2.4	160 ± 77
EJ	18	250 ± 39	120 ± 20	83 ± 20 a	7.0 ± 2.2 a	15 ± 11	8.9 ± 4.8	10 ± 9	8.9 ± 8.1	210 ± 122

Mean ± standard deviation. Means followed by different letters indicate the values were statistically different at $P < 0.05$ level among regions.

^a NS, North Sumatra; SS, Central and South Sumatra; WJ, West Java, EJ: Central and East Java.

^b TRB, total reverse in bases.

Table 3
Physicochemical and mineralogical properties of B horizon soils.

Region ^a	Total C	Total N	pH(H ₂ O)	Clay	Silt	Sand	Al _o + 1/2Fe _o ^b	Si _o /(Al _o - Al _p) ^b	Allo. ^c	Ferr. ^c	log(H ₄ SiO ₄ ⁰) ^d
	g kg ⁻¹			%			g kg ⁻¹		g kg ⁻¹	g kg ⁻¹	
NS	22.6 ± 33.3	2.0 ± 2.5	4.9 ± 0.3 a	32 ± 21	28 ± 15	40 ± 18	21.9 ± 23.9	0.38 ± 0.10b	59 ± 77	11 ± 9	-3.99 ± 0.16c
SS	17.6 ± 12.9	2.1 ± 1.9	5.0 ± 0.5 a	30 ± 24	31 ± 18	38 ± 26	28.6 ± 32.7	0.54 ± 0.09 ab	78 ± 108	19 ± 19	-3.74 ± 0.34 bc
WJ	30.4 ± 33.5	2.9 ± 3.6	5.3 ± 0.8 ab	35 ± 14	36 ± 8	29 ± 12	40.8 ± 37.2	0.47 ± 0.08 ab	103 ± 114	35 ± 22	-3.54 ± 0.18 ab
EJ	18.6 ± 15.4	1.6 ± 1.3	5.8 ± 0.6b	31 ± 22	36 ± 10	33 ± 16	34.5 ± 30.8	0.62 ± 0.18 a	92 ± 108	31 ± 16	-3.38 ± 0.27 a

Mean ± standard deviation. Means followed by different letters indicate the values were statistically different at $P < 0.05$ level among regions.

^a NS, North Sumatra; SS, Central and South Sumatra; WJ, West Java, EJ: Central and East Java.

^b Al_o + 1/2Fe_o, active Al and Fe; Si_o/(Al_o - Al_p), Si to Al ratio of short-range-order aluminosilicates.

^c Allo., allophane; Ferr., ferrihydrite.

^d H₄SiO₄⁰, H₄SiO₄⁰ activity in soil–water suspension.

Table 4
Factor loadings, eigenvalue and explained variance for each factor by factor analysis of climate and geochemical data.

	Factor 1	Factor 2	Factor 3	Factor 4
	Dry season intensity	Leaching	Parent material	Temperature
MAT ^a	-0.21	-0.04	-0.10	0.88
MAP	-0.10	0.95	-0.11	0.15
EP	0.01	0.92	-0.11	-0.29
EP in driest quarter	-0.64	0.57	0.08	0.12
H ₄ SiO ₄ ⁰ activity	0.79	-0.23	-0.05	0.19
pH	0.86	0.08	0.09	-0.09
Total Si	-0.06	0.07	0.85	0.36
Total Fe	0.49	0.13	-0.69	0.14
Total K	0.14	-0.23	0.72	-0.18
TRB	0.46	0.06	0.57	-0.30
Total C	-0.22	0.01	-0.01	-0.85
Eigenvalue	2.36	2.21	2.08	1.93
Explained variance %	21.5	20.1	18.9	17.5

^a MAT, mean annual temperature; MAP, mean annual precipitation; EP, excess precipitation; TRB, total reserve bases.

variance) had high positive loadings of pH and H₄SiO₄⁰ activity in soil–water suspension and a negative contribution of EPDQ. Because high EPDQ means continuous moist conditions and greater leaching, thereby yielding lower pH and H₄SiO₄⁰ activity, we interpret the first factor to dominantly represent desiccation intensity for the dry season. The second factor (20 % of explained variance) showed positive loadings with MAP and EP, which we attribute to leaching intensity. The third factor (19 % of explained variance) had positive loadings of Si and K and a negative loading of Fe, thereby indicating the nature of parent materials (felsic versus mafic). The fourth factor (18 %) had a high positive

loading with MAT and a high negative loading with total C, thereby being indicative of temperature, whereby high temperature enhances the decomposition of organic matter and reduces total C.

3.4. Active Al and Fe

The active Al and Fe contents (Al_o + 1/2 Fe_o) were not significantly different between regions (Table 3), and values >20 g kg⁻¹, one criterion for andic soil properties, were only found in the low-temperature sites at higher elevations (<21 °C corresponding to >1000 m asl) (Fig. 3a). The Al_o, Fe_o, and Si_o contents were negatively correlated with the temperature factor score (Table 5). The Fe_o was also positively correlated with the dry season intensity and parent material factors (Table 5), whereas Fe_d, corresponding to Fe in free Fe (hydr)oxides, was strongly correlated with the parent material factor. The Fe_o/Fe_d ratios, a measure of Fe (hydr)oxide crystallinity, were relatively high for all sites (0.47 ± 0.29), especially at high elevation sites (>1000 m asl), which indicates a high active Fe (e.g., ferrihydrite) content within the free Fe (hydr)oxide fraction at low temperature sites. The Fe_o/Fe_d ratios correlated negatively with the temperature factor and positively with the dry season intensity factor (Table 5).

The Si_o/(Al_o - Al_p) ratio representing the Si to Al ratio of SRO aluminosilicates was significantly higher at EJ versus NS (Tables 3 and S6). Because Si_o <1 to 2 g kg⁻¹ should not be considered significant due to the lack of specificity by acid-oxalate (Dahlgren 1994), the Si_o/(Al_o - Al_p) ratio was determined only for soils with Si_o > 1 g kg⁻¹ (Table S6). The Si_o/(Al_o - Al_p) ratio was correlated with the dry season intensity factor ($r_s = -0.74$, $P < 0.001$) (Table 5) as well as the variables that contributed to the factor (EPDQ: $r_s = -0.41$, $P < 0.05$; pH: $r_s = 0.58$, $P < 0.001$; and H₄SiO₄⁰ activity: $r_s = 0.65$, $P < 0.001$, Fig. 3b), whereas the ratio did not correlate with the other factors representing leaching, parent material and temperature (Table 5). For Sumatra sites (NS and

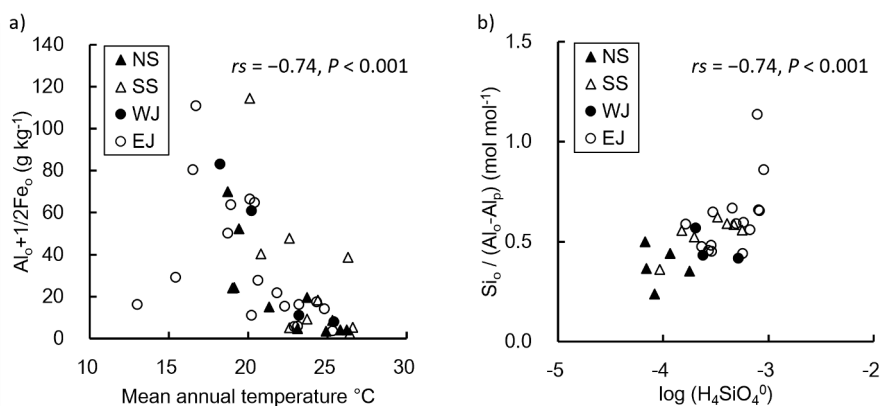


Fig. 3. Distribution of active Al and Fe (Al_o and Fe_o) and the ratio of Si to Al in short-range-order aluminosilicates (Si_o/(Al_o - Al_p)) in studied B horizon soils from regions under varied climatic and geochemical conditions. The sites with Si_o < 1 g kg⁻¹ were excluded in b. (NS, North Sumatra; SS, Central and South Sumatra; WJ, West Java, EJ: Central and East Java).

Table 5
Spearman correlation coefficients between factor scores and mineralogical properties of B horizon soils.

	Factor 1	Factor 2	Factor 3	Factor 4
	Dry season intensity	Leaching	Parent material	Temperature
Al _o ^a	0.10	0.20	-0.10	-0.81***
Fe _o	0.54***	0.15	-0.39*	-0.55***
Al _o + 1/2Fe _o	0.20	0.21	-0.15	-0.79***
Si _o	0.29	0.22	-0.07	-0.74***
Fe _d	0.14	0.19	-0.82***	0.20
Fe _o /Fe _d	0.33*	0.00	0.13	-0.78***
Al _p	-0.24	0.31*	0.05	-0.72***
Fe _p	-0.14	0.12	0.06	-0.63***
Si _o /(Al _o - Al _p)	0.74***	0.02	-0.05	0.28
Al _p /Al _o	-0.55***	0.12	0.09	0.23
Fe _p /Fe _o	-0.58***	0.00	0.33*	-0.10
Gibbsite	-0.54***	-0.26	-0.12	0.26
Kaolin	0.07	-0.06	-0.18	0.71***
Gibbsite/kaolin	-0.43**	-0.20	-0.06	-0.16
Smectite	0.31*	0.04	0.02	-0.14
Vermiculite	-0.65***	-0.13	0.04	-0.17
Mica	-0.39*	-0.23	0.35*	0.26

^a Al_o, Fe_o and Si_o, acid oxalate extractable Al, Fe, Si; Al_p and Fe_p, pyrophosphate extractable Al and Fe; Fe_d, dithionite-citrate extractable Fe.

Fe_o/Fe_d is an index of Fe oxide activity. Al_p/Al_o indicates organo-Al contribution to active Al fraction. Si_o/(Al_o - Al_p) is the Si to Al ratio in short-range-order minerals. Kaolin and gibbsite contents were determined by DTA. Smectite, vermiculite and mica were peak intensity in X-ray diffractogram of Mg-saturated specimen.

SS), 5 of the 12 soils had a Si_o/(Al_o - Al_p) ratio lower than 0.5, which is lower than the Si_o/(Al_o - Al_p) ratios known to exist for imogolite (0.5) and allophanes (0.5–1.0).

The Al_p and Fe_p fraction, which represents organically complexed Al and Fe, negatively correlated with the temperature factor (Table 5). The Al_p/Al_o and Fe_p/Fe_o ratios provide a measure for the proportion of organo-Al/Fe complexes in the total active Al/Fe fraction. Ratios higher than 0.5 indicate that organo-Al/Fe complexes are the predominant component of the active Al/Fe fraction (Candra et al., 2019). The Al_p/Al_o and Fe_p/Fe_o ratios of this study were relatively low for all the sites (0.19 ± 0.16 and 0.11 ± 0.13, respectively; Table S6), indicating low levels of Al/Fe-humus complexes relative to SRO Al/Fe minerals. The Al_p/Al_o and Fe_p/Fe_o ratios were negatively correlated with the dry season intensity factor, but not with the temperature factor, in contrast to Al_p and Fe_p (Table 5).

3.5. Crystalline clay minerals

XRD results for crystalline clay minerals (Fig. S2) are summarized in Table 6. There was a higher detection rate for gibbsite in Sumatra (7/9 sites for NS and 4/11 sites for SS) than Java (0/4 sites for WJ and 3/18 sites for EJ). Kaolin minerals (0.7-nm and 1.0-nm) were widely distributed and detected in most soils (Table 6). Kaolinite was more abundant than halloysite in soils from Java than Sumatra (Table 6). The detected halloysite was mainly in the hydrated (1.0 nm) form (Table 6), and halloysite (1.0 nm) was the dominant kaolin peak in 5/9 NS soils, 4/11 SS soils, and 4/18 EJ soils. Hydrated halloysite was dominant in soils with no distinct seasonal moisture deficit (EPDQ > 0 mm), especially those in Sumatra (Table 6). Conversely, 0.7-nm halloysite was predominantly found in soils at lower elevations of EJ (i.e., EJ1 and EJ3) having a distinct dry period and high H₄SiO₄⁰ activity in soil–water suspensions (log(H₄SiO₄⁰) = -3.18 and -3.09, respectively) (Tables 1, 3 and 6).

Vermiculite was abundant at Sumatra, especially at NS, where mica was also detected in both the clay- and silt-size fractions (Table 6). In contrast, neither vermiculite nor mica was found in the Java soils. Vermiculite and mica were preferentially found at sites with a low “Fe-Ti

vs Si-K” score reflecting the presence of felsic parent materials (Fig. 2). Mica peak detection was correlated with the parent material factor ($r_s = 0.35$, $P < 0.05$) and dry season intensity factor ($r_s = -0.35$, $P < 0.05$; Table 5). The occurrence of mica in felsic parent materials was suggested by the significant correlations of mica with total Si ($r_s = 0.35$, $P < 0.05$), total Fe ($r_s = -0.50$, $P < 0.001$), and total K ($r_s = 0.33$, $P < 0.05$). In contrast to mica, vermiculite detection was influenced by climate, with a negative correlation between vermiculite and the dry season intensity factor ($r_s = -0.65$, $P < 0.001$). Smectite was clearly detected in some Java soils (7/22), but not in Sumatra soils. Smectite was found in those Java soils with a distinct dry period (Table 6), demonstrated by a positive correlation with the dry season intensity factor (Table 5). Hydroxy-Al interlayering of 1.4-nm minerals was prominent. All vermiculite displayed evidence of hydroxy-Al interlayers, as demonstrated by the progressive collapse of the 1.4 nm peak in the K-saturated treatment to 1.0 nm upon heating to 350 and 550°C. Similarly, most of the detected smectite peaks displayed evidence of hydroxy-Al interlayering (Table 6).

Consistent with XRD characterization, the DTA results (Fig. S3) showed that gibbsite was more abundant in Sumatra versus Java soils (Table 6). The content of kaolin minerals was larger for the higher temperature sites at low elevations and strongly correlated with the temperature factor ($r_s = 0.71$, $P < 0.001$). In contrast, the content of kaolin minerals was small for soils with lower temperatures (<21°C) at elevations over 1000 m asl. The DTA-estimated gibbsite contents displayed a significant correlation with the dry season intensity factor ($r_s = -0.54$, $P < 0.001$), as well as variables that contributed to the factor (i.e., H₄SiO₄⁰ activity, EPDQ and pH; Fig. S5). The gibbsite content also had a positive correlation with total Al (Fig. S5). Moreover, the gibbsite/kaolin ratios were relatively higher in soils of Sumatra (especially NS) versus Java (Table 6) and were negatively correlated with the dry season intensity factor ($r_s = -0.43$, $P < 0.01$; Table 5).

3.6. Ion activities of soil–water suspension and stability diagrams for clay minerals

The pH value of soil–water suspensions for NS, SS, WJ and EJ soils ranged from 5.2 to 6.6, 4.6 to 7.5, 4.7 to 8.0, and 5.3 to 7.8, respectively. The pH of soil–water suspensions was relatively higher than soil pH (H₂O) for all regions, which may be due to the dissolution of minerals during the one-week equilibration period. The pH and H₄SiO₄⁰ activity were significantly higher at EJ (6.94 ± 0.58 and -3.38 ± 0.27) than NS (5.87 ± 0.43 and -3.99 ± 0.16) and SS (5.93 ± 0.83 and -3.74 ± 0.34) (Table S7). In contrast, Al³⁺ activity (log Al³⁺) was significantly lower at EJ than NS and SS owing to the higher pH values at EJ (Table S7). The H₄SiO₄⁰ activity displayed a negative correlation with EPDQ ($r_s = -0.51$, $P < 0.001$) and positive correlation with pH ($r_s = 0.50$, $P < 0.001$). Any potential relationships between ion activities (Al³⁺, H₄SiO₄⁰, and K⁺) and total elemental contents (parent materials) were indistinct (Fig. S4).

Smectite formation/stability was favorable in several soils based on thermodynamic considerations (Fig. 4). Soil solution composition was deemed to be saturated with respect to smectite (points lying on or above the smectite precipitation-dissolution line) for more than half of soil samples from EJ, WJ2, and WJ3 (Fig. 4a). Most soil solution activities were undersaturated with respect to amorphous Al(OH)₃ (33/42 sites) and Al-rich allophane (Si/Al = 0.5, 32/42 sites), and all the samples were undersaturated with respect to amorphous SiO₂. Supersaturation of soil solutions with respect to halloysite and kaolinite indicated these minerals could potentially form in all regions (Fig. 4a). The dissolution lines of gibbsite, imogolite, and kaolinite were close to the halloysite dissolution line, which indicated the potential formations of gibbsite, imogolite, and kaolinite in all regions.

We plotted solution activities within predominance-area fields of stability diagrams to demonstrate the relative stabilities of gibbsite, kaolinite, and muscovite (Fig. 4b) for the soils with mica and/or vermiculite in the clay fraction (Table 6). Most of the NS and SS soil solution activities were plotted within the gibbsite or kaolinite stability

Table 6
Mineralogical properties for crystalline minerals of B horizon soils.

Site	Elevation	Differential thermal analysis			X-ray diffraction analysis ^a							
		Gibbsite	Kaolin minerals	Gibbsite /kaolin ratio	Smectite	Vermiculite	Mica	Gibbsite	Kaolin minerals	Dominant kaolin peak ^{b c}	Identified 1.4-nm mineral ^{d e}	Silt mica
	m	g kg ⁻¹ clay	g kg ⁻¹ clay	mol _{Al} ¹ /mol _{Al} ¹								
North Sumatra (NS)												
NS1	110	101	790	0.2	-	+	+	++	+	1.0	HIV	+
NS2	210	23.6	900	0	-	-	-	+	++	1.0		-
NS3	340	37.4	900	0.1	-	-	+	+	++	0.7 k		+
NS4	600	616	310	3.3	-	+	-	++	+	0.7 k	HIV-V	-
NS5	680	203	730	0.5	-	+	+	++	+	1.0	V-HIV	+
NS6	1010	425	420	1.7	-	+	+	++	+	1.0	V-HIV	+
NS7	1350	14.3	4	5.4	-	++	-	-	±		HIV	-
NS8	1430	19.5	0	-	-	++	-	±	-		HIV	-
NS9	1520	341	370	1.5	-	+	+	++	+	1.0	V-HIV	+
Central and South Sumatra (SS)												
SS1	80	2.0	800	0	-	+	+	±	++	0.7 k	HIV-V	-
SS2	150	235	210	1.8	-	-	-	++	+	1.0		-
SS3	190	2.1	850	0	-	±	-	±	++	0.7 k		-
SS4	300	0.4	790	0	±	-	-	-	++	0.7 k		-
SS5	470	323	420	1.3	-	±	-	++	+	1.0		-
SS6	650	488	270	3	-	+	-	++	+	0.7 k	HIV	-
SS7	770	2.7	650	0	-	-	-	-	++	1.0		-
SS8	780	5.1	740	0	-	+	-	±	++	0.7 k	HIV	-
SS9	1100	3.9	450	0	±	-	-	-	+	1.0		-
SS10	1200	414	8	87	±	±	-	++	±			-
SS11	1420	0.1	9	0	-	-	-	-	-			-
West Java (WJ)												
WJ1	300	0	560	0	++	-	-	-	+	0.7 k	HIS-S	-
WJ2	650	1.3	520	0	++	-	-	-	+	0.7 k	HIS-S	-
WJ3	1210	0	13	0	±	-	-	-	±			-
WJ4	1500	0.8	4	0.4	±	±	-	-	+	0.7 k		-
Central and East Java (EJ)												
EJ1	290	2.3	870	0	-	-	-	-	++	0.7 h		-
EJ2	310	0.6	710	0	±	-	-	-	++	0.7 k		-
EJ3	410	57.7	770	0.1	±	-	-	++	+	0.7 h		-
EJ4	480	0	730	0	-	-	-	-	+	0.7 k		-
EJ5	620	3.4	930	0	-	-	-	±	++	0.7 k		-
EJ6	630	5.5	940	0	-	-	-	+	++	1.0		-
EJ7	710	0	810	0	+	-	-	-	++	1.0	S	-
EJ8	860	87.1	880	0.2	-	-	-	++	+	1.0		-
EJ9	1000	2	50	0.1	±	±	-	±	+	0.7 k		-
EJ10	1050	1.7	730	0	-	-	-	-	++	0.7 k		-
EJ11	1060	0.5	860	0	-	-	-	-	++	0.7 k		-
EJ12	1190	0	0	-	±	±	-	-	-			-
EJ13	1240	0	30	0	-	-	-	-	±			-
EJ14	1380	0.1	650	0	-	-	-	-	++	1.0		-
EJ15	1700	0.6	5	0.2	+	-	-	-	-		HIS	-
EJ16	1700	0	0	-	+	-	-	-	-		HIS	-
EJ17	1860	0	25	0	+	-	-	-	±		HIS, HIV	-
EJ18	2260	0	260	0	-	-	-	-	-			-

^a ++: clearly detected with dominant peak; +: clearly detected; ±: not clearly detected; -: not detected (based on the peak height for Mg²⁺ saturated slide).

^b 1.0, 1.0 nm halloysite peak was dominant in Mg²⁺ saturated slide; 0.7 k, 0.7 nm kaolinite peak was dominant in Mg²⁺ saturated slide; 0.7 h, 0.7 nm halloysite was identified but kaolinite peak was dominant in Mg²⁺ saturated slide (A separate clay aliquot was treated with formamide to identify 0.7 nm halloysite).

^c Influence of mica peak was considered by comparing the Mg²⁺ saturated sample with and without glycerol treatment, which sifts 1.0 nm halloysite peak to ~1.1 nm.

^d HIV, hydroxy-Al interlayered vermiculite; V, vermiculite; S, smectite; HIS, hydroxy-Al interlayered smectite.

^e HIV, a large part of the 1.4 nm peak remained after K and heat treatment up to 350°C; HIV-V, a large part of the peak remained after K treatment (air-dried), V-HIV, a small part of the peak remained after K treatment (air-dried).

fields (Fig. 4b), indicating that muscovite is unstable in these samples. In the stability diagram comparing gibbsite, kaolinite, and smectite (Fig. 4c), samples falling within the gibbsite stability field were mainly from NS, which had lower H₄SiO₄⁰ activities and higher gibbsite contents (>10 g kg⁻¹ clay) than the other soils (Table 6 and Fig. 4c). In contrast, kaolinite was the projected stable phase in SS and Java soils. Further, Fig. 4c shows that more than half of EJ soils and the WJ1 sample (EPDQ ≤ 0), where we detected smectite (Table 6), had high pH and high H₄SiO₄⁰ activities that were within or close to the smectite stability field, thereby indicating that smectite is relatively more stable than gibbsite and kaolinite.

4. Discussion

4.1. Climate, parent material and geochemical properties

The soil moisture regimes were best distinguished by EPDQ rather than MAP or EP, and intense desiccation of soils during the dry season (ustic) was only found in Java soils (Table 1). The significantly higher soil pH at EJ was associated with a distinct dry season, and the significant negative correlation between pH and EPDQ (Fig. S4) demonstrates the importance of seasonal desiccation in soil acidification. Furthermore, continuous leaching, suggested by high EPDQ, contributes to low H₄SiO₄⁰ activities (Fig. S4). Hence, EPDQ, pH, and H₄SiO₄⁰ activity were

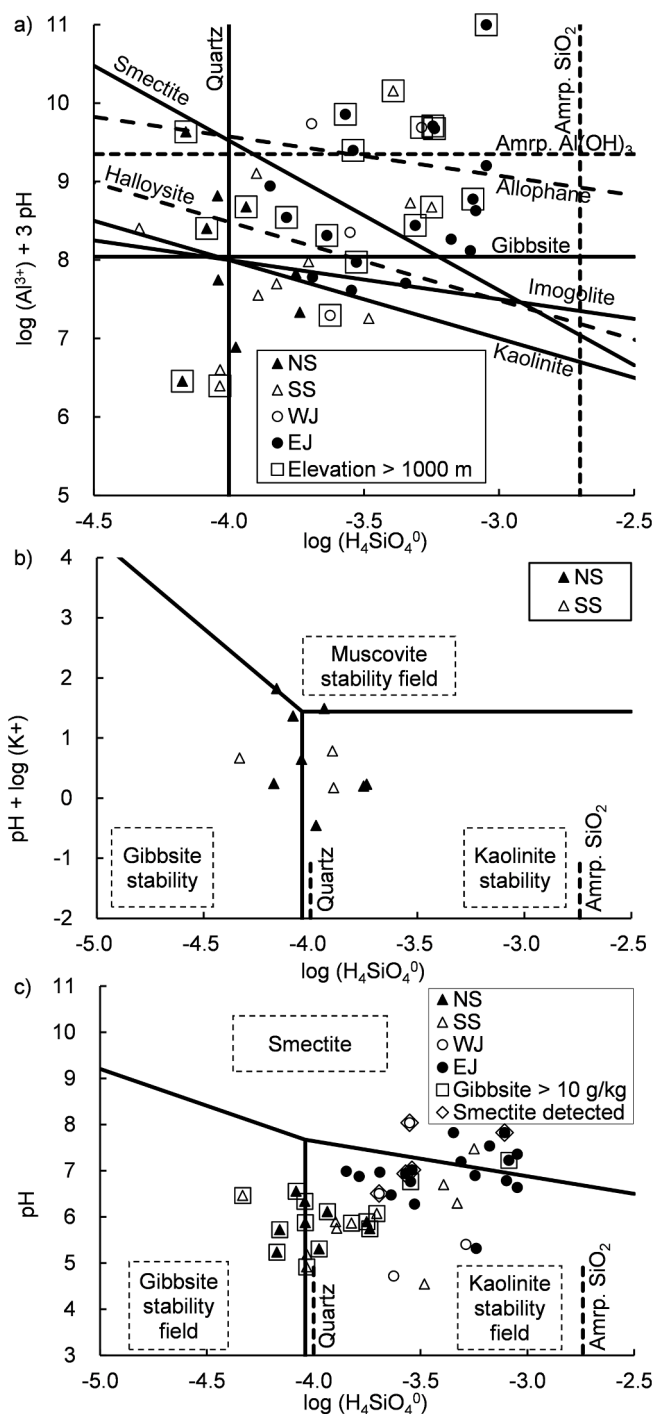


Fig. 4. Composition of the soil–water suspension of B horizon soil samples from different regions plotted on solubility (a) and stability (b and c) diagrams. Mean values of pH and ion activities for soil–water suspension used to draw the diagrams: $\text{pH} = 6.4$, $\log Mg^{2+} = -4.7$, $\log Fe^{3+} = -14.5$, $\log K^+ = -4.9$ (NS, North Sumatra; SS, Central and South Sumatra; WJ, West Java, EJ: Central and East Java).

all reflected in the dry season intensity factor (Table 4).

Total elemental composition retains some information on the original parent materials, although it also reflects weathering and soil formation processes (Watanabe et al. 2017, Lyu et al. 2018). The lower total Fe contents ($51 \pm 27 \text{ g kg}^{-1}$, Table 2) and the factor analysis diagram (Fig. 2) showed that the parent materials of NS were more felsic. The parent materials for SS, WJ, and EJ sites were considered intermediate to mafic based on their total Fe contents (Table 2); the average

Fe contents of andesitic and basaltic materials are 55 and 83 g kg^{-1} , respectively (Best, 2003). These results are consistent with the parent material information acquired from the geological maps of Sumatra and Java (Table S1): NS sites are rhyodacitic-to-andesitic, SS and Java sites are andesitic-to-basaltic (Amin et al., 1999; Gafoer et al., 1996; Gafoer et al., 2012; Gafoer and Ratman, 1999; Ratman and Gafoer, 1998). The presence of mica, a common primary mineral in felsic rocks, in the silt fraction of soils from NS by XRD (Table 6) further supports the felsic nature of parent materials from NS. The negative relationships between total Si and K versus total Fe (Table S4) were considered to reflect the nature of parent materials and were captured in the parent material factor (Table 4).

The degree of weathering along the temperature (elevation) gradient was not clear. For example, no correlation between MAT and total Si or TRB (Fig. S4) indicates that the degree of desilication and residual primary mineral contents were similar among soils across the wide temperature gradient ($13.0\text{--}26.6^\circ\text{C}$). However, a positive correlation between clay content and temperature (Fig. S4) does imply those higher temperatures at lower elevations may promote weathering. These contrasting trends may be associated with desilication and TRB incorporating both congruent and incongruent weathering processes, whereas clay formation is often dominated by incongruent weathering. The higher EP values at higher elevations may promote a greater degree of congruent weathering due to the greater leaching potential and also lower temperatures that inhibit the formation of crystalline clay minerals (Lyu et al., 2018).

4.2. Factors affecting contents and composition of SRO minerals

Temperature was identified as a strong control on the distribution of SRO minerals (Al_o , Fe_o and Si_o), as well as organo-Al/Fe components (Al_p and Fe_p) in the humid tropical volcanic regions of Indonesia (Table 5, Fig. S5). These components (Al_o , Fe_o , Si_o , Al_p and Fe_p) displayed significant negative correlations with the temperature factor rather than the dry season intensity, leaching, and parent material factors (Table 5). Notably, soil samples from the low-temperature sites ($<21^\circ\text{C}$) met the criterion of andic soil properties ($Al_o + 1/2Fe_o > 20 \text{ g kg}^{-1}$) (Fig. 3a). The negative correlation between the Fe_o/Fe_d ratio and temperature factor ($r_s = -0.78$, $P < 0.001$) indicates a higher fraction of SRO ferrihydrite within the total free Fe (hydr)oxide pool at sites with lower temperatures. Additionally, total C negatively contributed to the temperature factor (Table 4) and, therefore, positively related to the content of Al_o , Fe_o , Al_p and Fe_p (Fig. S5). These results indicate that the temperature mainly regulates the quantity of active Al and Fe rather than parent material and moisture conditions. The low temperature retards the crystallization of clay minerals (e.g., kaolinite and smectite), thereby promoting the formation of kinetically favored but metastable SRO minerals, such as ferrihydrite, allophane, and imogolite (Lyu et al., 2018; Rasmussen et al., 2010; Rasmussen et al., 2007). The higher organic matter concentrations resulting from slower decomposition rates at lower temperatures promote the formation of organo-Al/Fe complexes by providing additional functional groups for metal complexation. Also, the high organic matter content at the lower temperature, higher elevation sites may retard the crystallization of crystalline clay minerals (e.g., gibbsite and kaolinite) by interfering with crystallization (e.g., organic sorption inhibiting crystallization on mineral surfaces) (Huang et al., 2002; Schwertmann, 1985).

The Al_o and Si_o were abundant at low temperature - high elevation sites (Fig. 4a and S5), partly due to the supersaturation of soil solution activities with respect to SRO aluminosilicates, such as allophane and imogolite. The rapid kinetics of nucleation for SRO minerals favor the formation of these metastable solid phases relative to their more thermodynamically stable crystalline mineral equivalents (Stumm, 1992). The “aging” or “Ostwald Ripening” process (i.e., transformation of non- and nano-crystalline phases to crystalline phases via dissolution and reprecipitation) is typically a slow process due to the small differences in

free energy between the two phases (Stumm, 1992). Climatic conditions play an important role in the formation of crystalline minerals as crystallization is promoted as the soil climate becomes warmer (Schwertmann, 1985; Talibudeen, 1981).

The influence of soil moisture conditions on active Al and Fe contents was less evident than the temperature. Active Al and Fe components (Al_o , Fe_o , Al_p and Fe_p) were not correlated with the leaching factor or MAP (Table 5), though EP showed some correlations (Fig. S5). Whereas a distinct dry season (e.g., ustic) hinders neoformation of active Al and Fe components by limiting the release of Al and Fe from weathering of the parent material during the extended dry period (Georgoulas and Moustakas, 2010), it was not evident in the studied soils, sharply contrasting with previous research in volcanic soils of drier regions (e.g., California (Rasmussen et al. 2007, Rasmussen et al. 2010), Hawaii (Chadwick et al. 2003), Tanzania (Lyu et al. 2018), Galapagos (Candra et al. 2019)). The lack of influence may come from the fact that most of the sites had sufficient moisture throughout the year (MAP > 1900 mm).

The dry season intensity influenced the Si to Al ratio of SRO aluminosilicates, $Si_o/(Al_o - Al_p)$. The correlation between the dry season intensity factor and $Si_o/(Al_o - Al_p)$ suggests that the Si to Al ratio is controlled by $H_4SiO_4^0$ activity (Fig. 3b), which was, in turn, strongly affected by EPDQ (Fig. S4). The more intense leaching at sites with high EP throughout the entire year (e.g., NS sites) reduced the $H_4SiO_4^0$ activity, enhancing the formation of Al-rich allophane with a low Si/Al ratio (Candra et al., 2019). Five out of 12 of Sumatra sites with $Si_o > 1$ g kg^{-1} had a $Si_o/(Al_o - Al_p)$ ratio lower than 0.5, which is below the lowest ratios reported for allophane (0.5–1) and imogolite (0.5) (Harsh et al., 2002). This apparent discrepancy may result from acid-oxalate extracting Al from Al-hydroxides (e.g., gibbsite, hydroxy-Al interlayers of 2:1 layer silicates) found at sites without a distinct seasonal dry period.

Additionally, the Al_p/Al_o ratio and Fe_p/Fe_o ratio were high in the soils without a distinct dry season and with a low pH (Table 5 and Fig. S5). A persistently high moisture status led to leaching of base cations, resulting in low pH (<5), which increases Al^{3+}/Fe^{3+} activities and impedes organic matter decomposition (Table 4, Figs. S4 and S5), collectively promoting the formation of organo-Al/Fe complexes (Candra et al., 2019; Parfitt and Kimble, 1989) at the expense of SRO aluminosilicates and ferrihydrite, the so-called anti-allophanic effect (Shoji et al., 1993). Furthermore, low pH condition promotes complexation of partially-decomposed organic matter and variable charge mineral surfaces with strong innersphere bonds (Kleber et al., 2015), thereby contributing to stabilization and accumulation of organic matter.

Furthermore, higher $H_4SiO_4^0$ activities, found in soils with a distinct dry season, can inhibit the crystallization of active Fe components, as suggested by the positive correlation of the dry season intensity factor with Fe_o and Fe_o/Fe_d (Table 5). Higher $H_4SiO_4^0$ activities increase Si sorption on Fe (hydr)oxide surfaces that block/impede sites for further Fe precipitation, thereby inhibiting the crystallization of ferrihydrite to goethite/hematite (Anderson and Benjamin, 1985; Francisco et al., 2016).

The nature of parent material did not show a clear influence on active Al and Fe. The strong correlation of the parent material factor with Fe_d ($r_s = -0.82$, $P < 0.001$), but weak correlation with Fe_o ($r_s = -0.39$, $P < 0.05$; Table 5) suggest high free Fe (hydr)oxide content was found in the soils with mafic nature, but the crystallinity of Fe (hydr) oxides seems more controlled by the temperature and dry season intensity.

4.3. Factors affecting neoformation and transformation of crystalline clay minerals

Moisture conditions, especially during the dry season, appear to play a disproportionate role in controlling the neoformation of crystalline clay minerals. Negative correlations of gibbsite content with the dry season intensity factor (Table 5) and the $H_4SiO_4^0$ activity of soil-water

suspensions (Fig. S5) and a negative correlation of the gibbsite/kaolin ratio with the dry season intensity factor (Table 5) suggest that the low $H_4SiO_4^0$ activity caused by continuous leaching is favorable for the neoformation of gibbsite versus kaolin minerals (Huang et al., 2002; Lyu et al., 2018). Soils at NS sites had low $H_4SiO_4^0$ activities due to the continuous high leaching intensity, and gibbsite is considered to be the most stable clay mineral in this low H_4SiO_4 soil environment (Fig. 4c). Moreover, a high supply of Al from weathering of primary minerals and SRO aluminosilicates promotes the neoformation of gibbsite, as supported by the positive correlation between the contents of gibbsite and total Al (Fig. S5).

Kaolin minerals (i.e., kaolinite and halloysite) formation is favored at low elevation sites (<1000 m asl) with higher temperatures. The content of kaolin minerals was positively correlated with the temperature factor (Table 5) and negatively correlated with TRB, which is an indicator of the degree of primary mineral weathering (Fig. S5). The higher temperatures at low elevation sites promote weathering and the crystallization of kaolin minerals at the expense of SRO aluminosilicates and primary minerals (Lyu et al., 2018; Rasmussen et al., 2010; Watanabe et al., 2017). Kaolin minerals were more widely distributed than gibbsite, which is consistent with the solubility and stability diagrams (Fig. 4a and 4c, respectively), indicating that kaolinite is more stable than gibbsite at the existing soil solution ion activities for many of the soils.

Concerning kaolin mineral species, the hydrated halloysite (1.0 nm) was found in soils with no distinct seasonal moisture deficit, especially those in Sumatra (Table 6). The neoformation of halloysite generally requires continuous moist conditions, high $H_4SiO_4^0$ activity, and acidic pH values. Under acidic conditions, the octahedral sheet has a positive charge opposite to that of the tetrahedral sheet, which results in incorporation of two interlayer H_2O molecules between the 1:1 units yielding a 1.0 nm halloysite structure (Churchman et al., 2016). Interestingly, we found halloysite in soils having low $H_4SiO_4^0$ activity as opposed to the general concept that halloysite forms under high $H_4SiO_4^0$ activity (Churchman and Lowe, 2012). Preferential formation of halloysite in soils of volcanic parent materials has been shown to occur when $H_4SiO_4^0$ activity in the soil solution was $\geq 10^{-3.45}$ mol L^{-1} (Singleton et al., 1989; Takahashi et al., 1993). Locally high $H_4SiO_4^0$ activity in the soil might allow the formation of halloysite, and the halloysite presence may be kinetically favored versus more crystalline minerals (Kautz and Ryan, 2003; Ziegler et al., 2003).

Kaolinite was more abundant at Java sites than halloysite (Table 6). Kaolinite appears to preferentially form under moist conditions with a distinct dry season (Churchman et al., 2010) in Java soils (Tables 1 and 6). Additionally, dehydrated halloysite (0.7 nm expandable to 1.0 nm with formamide) was found at EJ (EJ1 and EJ3), which has a distinct dry season and high $H_4SiO_4^0$ activity (Tables 1, 3, and 4). The solubility diagram (Fig. 4a) demonstrates favorable halloysite formation in these soils. Though we applied the formamide test to detect halloysite, independently quantifying halloysite versus kaolinite in soil samples is still a challenging task, and some tubular forms of halloysite do not expand with formamide (Joussein et al., 2005). The distinct drying in EJ soils may facilitate dehydration of 1.0 nm halloysite to the 0.7 nm form. In the xeric moisture regime of northern California, halloysite (1.0 nm with or without formamide treatment) and kaolinite (0.7 nm with formamide) concentrations show an inverse relationship with depth, with the content of halloysite increasing down the profile (Takahashi et al., 2001). The kaolinite in the surface horizons had the same tubular morphology as the halloysite at depth, suggesting that hydrated halloysite transforms to kaolinite upon dehydration during the summer period of soil profile desiccation (Takahashi et al., 2001). Halloysite formation under relatively high $H_4SiO_4^0$ activity may also compete with Si-rich allophane formation, with temperature determining the crystallinity of the resulting precipitate (Churchman and Lowe, 2012; Joussein et al., 2005).

Halloysite and smectite formation are both favored by high $H_4SiO_4^0$

activity, but smectite tends to be the favored product in base-rich and higher pH environments. Smectite was found in the soils with lower leaching intensities (i.e., EJ and WJ soils, Table 6). Although the solubility diagram (Fig. 4a) indicates that smectite formation is possible in most EJ and WJ sites, smectite was detected in only a limited number of soils (Table 6). The lack of smectite may result from smectite being a metastable phase relative to kaolin minerals (Fig. 4c), the difficulty of detecting trace levels of neoformed smectite (van der Gaast et al., 1986), and/or preferential formation of kinetically-favored SRO minerals. The distribution of smectite was consistent with the stability diagram fields (Fig. 4c), which showed that smectite is the most stable clay mineral under current soil solution ion activities. The presence of smectite was positively correlated with the dry season intensity factor (Table 5), indicating that high $H_4SiO_4^0$ activity and pH in soils with intense desiccation promote smectite formation. The seasonal desiccation of soils may further promote the neoformation of smectite by increasing ion activities (by reducing leaching and dry season evapo-concentration) and enhancing the crystallization of secondary minerals as a result of dehydration. Conversely, the persistently moist conditions at NS and SS (having high positive EPDQ) appear to inhibit smectite formation due to the higher leaching intensity reducing both pH and $H_4SiO_4^0$ activity (Watanabe et al., 2017).

Vermiculite originates as a transformation product from mica, which occurs in felsic parent materials containing mica as a precursor primary mineral. The correlations of mica detection with total Si, K, and Fe ($r_s = 0.35$, $P < 0.05$; $r_s = 0.33$, $P < 0.05$; $r_s = -0.50$, $P < 0.001$; respectively) and the prevalent detection of mica in the silt fraction of all NS soils indicate that mica was inherited from the felsic parent material and serves as a precursor to vermiculite (Bailey et al., 1988). The stability diagram (Fig. 4b) indicates the instability of mica (muscovite) in NS soils. The negative correlation between vermiculite detection with the dry season intensity factor also suggests vermiculite formation under continuous leaching conditions, such as NS soils. The continuous leaching likely enhances soil acidification and loss of base elements (Rowell and Wild, 1985), which results in low pH and K^+ activities in NS soils. Mica alteration involving K^+ removal results in the formation of an expandable 2:1 type mineral (i.e., vermiculite) as a transitional product (Churchman and Lowe, 2012; Watanabe et al., 2006).

Hydroxy-Al interlayering was common in all vermiculite specimens in NS soils (Table 6). Given an abundant supply of Al from primary mineral weathering (rapid weathering of glass-rich tephra), moderately acidic pH values, and the high temperature in tropical regions ($MAT > 18^\circ C$ for NS sites), the formation of hydroxy-Al interlayering is promoted in the 2:1 layer silicates (Carstea, 1968; Ndayiragije and Delvaux, 2003). The deposition of hydroxy-Al polymers (gibbsite-like crystals) in inter-layer position of 2:1 layers silicates is a common feature in moderately acidic (~5.0) soil environments and has been termed the anti-gibbsite effect (Jackson, 1963; Jackson, 1964), as it may inhibit gibbsite formation as a separate phase. Hydroxy-Al interlayering of 2:1 layer silicates is reported to reduce their susceptibility to alteration and increase their thermodynamic stability (Karathanasis, 2002).

5. Conclusion

Climatic factors (temperature and dry season intensity) primarily controlled the distribution of soil secondary minerals in combination with parent materials (felsic or mafic tephra) that determine contents of free Fe (hydr)oxides and mica. The active Al and Fe fraction was predominant at high elevations, reflecting the importance of low temperature and continuous leaching in controlling the formation of organo-Al/Fe complexes and SRO minerals.

The moisture status during the dry season (EPDQ) was identified as an important control on the Si/Al ratio of secondary minerals via regulation of elemental activities in soil solutions. Low $H_4SiO_4^0$ activity under continuous leaching (i.e., high EPDQ) resulted in a low Si/Al ratio of SRO aluminosilicates and the formation of gibbsite. Conversely, high

$H_4SiO_4^0$ activity resulting from intense desiccation (low EPDQ) enhances the formation of SRO aluminosilicates with a high Si/Al ratio (Si-rich allophane) and smectite. Furthermore, the lower pH associated with continuously high moisture conditions promotes the formation of organo-Al/Fe complexes. In addition, vermiculite transformation from mica derived from felsic parent materials occurred in NS soils under conditions of low pH and K^+ activity caused by a continuous leaching regime.

This study elucidated the importance of temperature and dry season intensity as the primary controlling factors for the distribution of active Al and Fe (organo-metal complexes and SRO minerals) and crystalline minerals in volcanic parent materials of the humid tropics. Considering that the distribution of secondary minerals controls nutrient dynamics (P sorption/CEC), organic matter accumulation, porosity/water holding characteristics, soil tilth, etc., information regarding clay mineral distributions from this study contributes to agricultural and environmental management in humid volcanic regions.

Declaration of Competing Interest

The authors declare that they have no known competing financial interests or personal relationships that could have appeared to influence the work reported in this paper.

Data availability

Data will be made available on request.

Acknowledgment

This work was supported by the JSPS KAKENHI Grant Numbers 17H06171, 20H04322, and 20KK0261.

Appendix A. Supplementary data

Supplementary data to this article can be found online at <https://doi.org/10.1016/j.geoderma.2022.116058>.

References

- Amin, T.C., Ratman, N., Gafoer, S., 1999. Geological Map of Middle Part of Java, Regional Geological Map. Geological Research and Development Centre.
- Anda, M., Dahlgren, R.A., 2020. Mineralogical and surface charge characteristics of Andosols experiencing long-term, land-use change in West Java, Indonesia. *Soil Sci. Plant Nutr.* 66 (5), 702–713.
- Anderson, P.R., Benjamin, M.M., 1985. Effect of silicon on the crystallization and adsorption properties of ferric oxides. *Environ. Sci. Technol.* 19 (11), 1048–1053.
- Asano, M., Wagai, R., 2014. Evidence of aggregate hierarchy at micro- to submicron scales in an allophanic Andisol. *Geoderma* 216, 62–74.
- Bailey, S.W., de la Calle, C., Suquet, H., 1988. Chapter 12. VERMICULITE. In: S.W. Bailey (Ed.), *Hydrous Phyllosilicates*. De Gruyter, pp. 455–496.
- Best, M.G., 2003. *Igneous and metamorphic petrology*. John Wiley & Sons.
- Blakemore, L.C., 1987. Extractable iron, aluminium and silicon. In *methods for chemical analysis of soils*. NZ Soil Bureau Scientific Report 80, 71–76.
- Buol, S.W., Southard, R.J., Graham, R.C., McDaniel, P.A., 2011. *Soil genesis and classification*. John Wiley & Sons.
- Candra, I.N., Gerzabek, M.H., Ottner, F., Tintner, J., Wriessnig, K., Zehetner, F., 2019. Weathering and soil formation in rhyolitic tephra along a moisture gradient on Alcedo Volcano, Galápagos. *Geoderma* 343, 215–225.
- Carstea, D.D., 1968. Formation of hydroxy-Al and -Fe interlayers in montmorillonite and vermiculite - influence of particle size and temperature. *Clays Clay Miner.* 16 (3), 231–238.
- Chadwick, O.A., Gavenda, R.T., Kelly, E.F., Ziegler, K., Olson, C.G., Elliott, W.C., Hendricks, D.M., 2003. The impact of climate on the biogeochemical functioning of volcanic soils. *Chem. Geol.* 202, 195–223.
- Childs, C.W., 1985. *Towards understanding soil mineralogy II. Notes on ferrihydrite*. N.Z. Soil Bureau Laboratory Report CM7. Department of Scientific and Industrial Research.
- Churchman, G.J., Lowe, D.J., 2012. Alteration, formation, and occurrence of minerals in soils. In: P.M. Huang, L. Y., M.E. Sumner (Eds.), *Handbook of Soil Science Properties and Processes*. CRC Press.
- Churchman, G.J., Whitton, J.S., Claridge, G.G.C., Theng, B.K.G., 1984. Intercalation method using formamide for differentiating halloysite from kaolinite. *Clays Clay Miner.* 32 (4), 241–248.

- Churchman, G.J., Pontifex, I.R., McClure, S.G., 2010. Factors influencing the formation and characteristics of halloysites or kaolinites in granitic and tuffaceous saprolites in Hong Kong. *Clays Clay Miner.* 58 (2), 220–237.
- Churchman, G.J., Pasbakhsh, P., Lowe, D.J., Theng, B.K.G., 2016. Unique but diverse: some observations on the formation, structure and morphology of halloysite. *Clay Miner.* 51 (3), 395–416.
- Crow, M., Barber, A., 2005. Map: Simplified geological map of Sumatra. Geological Society of London, London.
- Cunningham, M.J., Lowe, D.J., Wyatt, J.B., Moon, V.G., Churchman, G.J., 2016. Discovery of halloysite books in altered silicic Quaternary tephras, northern New Zealand. *Clay Miner.* 51 (3), 351–372.
- Dahlgren, R., 1994. Quantification of Allophane and Imogolite. In: Amonette, J.E., Stucki, J.W. (Eds.), *Quantitative Methods in Soil Mineralogy*. Soil Science of America Inc, Madison, WI, USA, pp. 430–451.
- Dahlgren, R.A., Ugolini, F.C., 1989. Formation and stability of imogolite in a tephritic Spodosol, Cascade Range, Washington, U.S.A. *Geochim. Cosmochim. Acta* 53 (8), 1897–1904.
- Dahlgren, R.A., Saigusa, M., Ugolini, F.C., 2004. The nature, properties and management of volcanic soils. *Adv. Agron. Academic Press* 113–182.
- Del Grosso, S., Parton, W., Stohlgren, T., Zheng, D., Bachelet, D., Prince, S., Hibbard, K., Olson, R., 2008. Global potential net primary production predicted from vegetation class, precipitation, and temperature. *Ecology* 89 (8), 2117–2126.
- Delvaux, B., Herbillon, A.J., Vielvoye, L., 1989. Characterization of a weathering sequence of soils derived from volcanic ash in Cameroon. *Taxonomic, mineralogical and agronomic implications*. *Geoderma* 45 (3), 375–388.
- Driscoll, C.T., 1984. A procedure for the fractionation of aqueous aluminum in dilute acidic waters. *Int. J. Environ. Anal. Chem.* 16 (4), 267–283.
- Fick, S.E., Hijmans, R.J., 2017. WorldClim 2: new 1-km spatial resolution climate surfaces for global land areas. *Int. J. Climatol.* 37 (12), 4302–4315.
- Francisco, P.C.M., Sato, T., Otake, T., Kasama, T., 2016. Kinetics of Fe³⁺ mineral crystallization from ferrihydrite in the presence of Si at alkaline conditions and implications for nuclear waste disposal. *Am. Mineral.* 101 (9), 2057–2069.
- Gafoer, S., Amin, T.C., Samodra, H., 1996. Geological Map of Indonesia, Medan Sheet, Systematic Geological Map of Indonesia. Geological Research and Development Centre.
- Gafoer, S., Amin, T.C., Setyogroho, B., 2012. Geological Map of Indonesia, Palembang Sheet, Systematic Geological Map of Indonesia. Geological Research and Development Centre.
- Gafoer, S., Ratman, N., 1999. Geological Map of Eastern Part of Java. Regional Geological Map, Geological Research and Development Centre.
- Gee, G.W., Or, D., 2002. 2.4 Particle-Size Analysis. In: J.H. Dane, G.C. Topp (Eds.), *Methods of Soil Analysis*. SSSA Book Series, pp. 255–293.
- Georgoulas, F.A., Moustakas, N.K., 2010. Exploration of soils developing on volcanic materials on the island of Milos, Greece. *Catena* 81 (1), 43–54.
- Global-Volcanism-Program, 2013. *Volcanoes of the World*, v. 4.11.0. In: E. Venzke (Ed.), Smithsonian Institution.
- Gustafsson, J.P., 2014. Visual MINTEQ 3.1. Stockholm: KTH, Department of Land Water Resources Engineering.
- Harris, W., White, G.N., 2008. X-ray Diffraction Techniques for Soil Mineral Identification. In: A.L. Ulery, L. Richard Drees (Eds.), *Methods of Soil Analysis Part 5—Mineralogical Methods*. SSSA Book Series. Soil Science Society of America, Madison, WI, pp. 81–115.
- Harsh, J., Chorover, J., Nizeyimana, E., 2002. Allophane and Imogolite, Soil Mineralogy with Environmental Applications. SSSA Book Series, pp. 291–322.
- Hossner, L., 1996. Dissolution for total elemental analysis. *Methods of Soil Analysis Part 3—Chemical Methods*, 49–64.
- Huang, Y.-T., Lowe, D.J., Churchman, G.J., Schipper, L.A., Cursons, R., Zhang, H., Chen, T.-Y., Cooper, A., 2016. DNA adsorption by nanocrystalline allophane spherules and nanoaggregates, and implications for carbon sequestration in Andisols. *Appl. Clay Sci.* 120, 40–50.
- Huang, P.M., Wang, M.K., Kämpf, N., Schulze, D.G., 2002. Aluminum Hydroxides. In: J. B. Dixon, D.G. Schulze (Eds.), *Soil Mineralogy with Environmental Applications*. SSSA Book Series. Soil Science Society of America, Madison, WI, pp. 261–289.
- Jackson, M.L., 1963. Aluminum bonding in soils: a unifying principle in soil science. *Proceed. Soil Sci. Soc. Am.* 27 (1), 1–10.
- Jackson, M.L., 1964. Chemical composition of soils. In: Bear, F. (Ed.), *Chemistry of the Soil*. Van Nostrand-Reinhold, New York, pp. 71–141.
- Joussein, E., Petit, S., Churchman, J., Theng, B., Righi, D., Delvaux, B., 2005. Halloysite clay minerals — a review. *Clay Miner.* 40 (4), 383–426.
- Karathanasis, A.D., 2002. Mineral Equilibria in Environmental Soil Systems. In: Dixon, J. B., Schulze, D.G. (Eds.), *Soil Mineralogy With Environmental Applications*. Soil Science Society of America, Madison, WI, SSSA Book Series, pp. 109–151.
- Kautz, C.Q., Ryan, P.C., 2003. The 10 Å to 7 Å halloysite transition in a tropical soil sequence, Costa Rica. *Clays Clay Miner.* 51 (3), 252–263.
- Kleber, M., Eusterhues, K., Keillweit, M., Mikutta, C., Mikutta, R., Nico, P.S., 2015. Chapter One – Mineral-Organic Associations: Formation, Properties, and Relevance in Soil Environments. *Adv. Agron.* 130, 140.
- Lindsay, W.L., 1979. *Chemical Equilibria in Soils*. John Wiley and Sons Ltd.
- Lyu, H., Watanabe, T., Kilasara, M., Funakawa, S., 2018. Effects of climate on distribution of soil secondary minerals in volcanic regions of Tanzania. *Catena* 166, 209–219.
- Lyu, H., Watanabe, T., Zhong, R., Kilasara, M., Hartono, A., Funakawa, S., 2021. Factors controlling sizes and stabilities of subsoil organic carbon pools in tropical volcanic soils. *Sci. Total Environ.* 769, 144842.
- Ndayiragije, S., Delvaux, B., 2003. Coexistence of allophane, gibbsite, kaolinite and hydroxy-Al-interlayered 2: 1 clay minerals in a perudic Andosol. *Geoderma* 117 (3–4), 203–214.
- Parfitt, R.L., 1990. Allophane in New Zealand—A review. *Aust. J. Soil Res.* 28 (3), 343–360.
- Parfitt, R.L., Kimble, J.M., 1989. Conditions for formation of allophane in soils. *Soil Sci. Soc. Am. J.* 53 (3), 971–977.
- Pennock, D., Yates, T., Braidek, J., 2007. *Soil sampling designs, Soil Sampling and Methods of Analysis*, pp. 1–14.
- Rasmussen, C., Matsuyama, N., Dahlgren, R.A., Southard, R.J., Brauer, N., 2007. Soil genesis and mineral transformation across an environmental gradient on andesitic lahar. *Soil Sci. Soc. Am. J.* 71 (1), 225–237.
- Rasmussen, C., Dahlgren, R.A., Southard, R.J., 2010. Basalt weathering and pedogenesis across an environmental gradient in the southern Cascade Range, California, USA. *Geoderma* 154 (3–4), 473–485.
- Ratman, N., Gafoer, S., 1998. *Geological Map of Western Part of Java, Regional Geological Map*. Geological Research and Development Centre.
- Rowell, D.L., Wild, A., 1985. Causes of soil acidification: a summary. *Soil Use Manag.* 1 (1), 32–33.
- Schwertmann, U., 1985. The Effect of Pedogenic Environments on Iron Oxide Minerals. In: Stewart, B.A. (Ed.), *Advances in Soil Science*. Springer, New York, New York, NY, pp. 171–200.
- Sharma, A., Weindorf, D.C., Wang, D.D., Chakraborty, S., 2015. Characterizing soils via portable X-ray fluorescence spectrometer: 4. Cation exchange capacity (CEC). *Geoderma* 239, 130–134.
- Shoji, S., Nanzyo, M., Dahlgren, R.A., 1993. Volcanic ash soils: genesis, properties and utilization. *Developments in Soil Science*, Elsevier, Amsterdam.
- Shoji, S., Takahashi, T., 2002. Environmental and agricultural significance of volcanic ash soils. *Global Environ. Res.* 6, 113–135.
- Siebert, L., Simkin, T., Kimberly, P., 2011. *Volcanoes of the World*. Univ of California Press.
- Sigfusson, B., Gislason, S.R., Paton, G.I., 2008. Pedogenesis and weathering rates of a Histic Andosol in Iceland: Field and experimental soil solution study. *Geoderma* 144 (3), 572–592.
- Singh, M., Sarkar, B., Biswas, B., Bolan, N.S., Churchman, G.J., 2017. Relationship between soil clay mineralogy and carbon protection capacity as influenced by temperature and moisture. *Soil Biol. Biochem.* 109, 95–106.
- Singleton, P., McLeod, M., Percival, H., 1989. Allophane and halloysite content and soil solution silicon in soils from rhyolitic volcanic material, New Zealand. *Soil Res.* 27 (1), 67–77.
- Soil Survey Staff, 2014. *Keys to Soil Taxonomy*, 12th ed. USDA-Natural Resources Conservation Service, Washington, DC.
- Stumm, W., 1992. Chemistry of the solid-water interface: processes at the mineral-water and particle-water interface in natural systems. John Wiley & Sons.
- Takahashi, T., Dahlgren, R., van Susteren, P., 1993. Clay mineralogy and chemistry of soils formed in volcanic materials in the xeric moisture regime of northern California. *Geoderma* 59 (1), 131–150.
- Takahashi, T., Dahlgren, R.A., 2016. Nature, properties and function of aluminum-humus complexes in volcanic soils. *Geoderma* 263, 110–121.
- Takahashi, T., Dahlgren, R.A., Theng, B.K.G., Whitton, J.S., Soma, M., 2001. Potassium-selective, halloysite-rich soils formed in volcanic materials from Northern California. *Soil Sci. Soc. Am. J.* 65 (2), 516–526.
- Takahashi, T., Shoji, S., 1996. Active aluminum status in surface horizons showing continuous climosequence of volcanic ash-derived soils in Towada district, northeastern Japan. *Soil Sci. Plant Nutr.* 42 (1), 113–120.
- Talibudeen, O., 1981. Precipitation. In: Greenland, D.J., Hayes, M.H.B. (Eds.), *The Chemistry of Soil Processes*. John Wiley & Sons, New York, pp. 81–114.
- Thorntwaite, C.W., 1948. An approach toward a rational classification of climate. *Geogr. Rev.* 38 (1), 55–94.
- Tsai, C.C., Chen, Z.S., Kao, C.I., Ottner, F., Kao, S.J., Zehetner, F., 2010. Pedogenic development of volcanic ash soils along a climosequence in Northern Taiwan. *Geoderma* 156 (1–2), 48–59.
- Van Breenen, N., Brinkman, R., 1976. Chemical equilibria and soil formation. *Dev. Soil Sci.* 5, 141–170.
- van der Gaast, S.J., Mizota, C., Jansen, J., 1986. Curved smectite in soils from volcanic ash in Kenya and Tanzania: a low-angle X-ray powder diffraction study. *Clays Clay Miner.* 34 (6), 665–671.
- Van Ranst, E., Utami, S.R., Shamshuddin, J., 2002. Andisols on volcanic ash from Java Island, Indonesia: Physico-chemical properties and classification. *Soil Sci.* 167 (1), 68–79.
- Van Ranst, E., Utami, S., Verdoodt, A., Qafoku, N., 2008. Mineralogy of a perudic Andosol in central Java, Indonesia. *Geoderma* 144 (1–2), 379–386.
- Van Ranst, E., Kips, P., Mbogoni, J., Mees, F., Dumon, M., Delvaux, B., 2020. Halloysite-smectite mixed-layered clay in fluvio-volcanic soils at the southern foot of Mount Kilimanjaro, Tanzania. *Geoderma* 375, 114527.
- Vingiani, S., Righi, D., Petit, S., Terribile, F., 2004. Mixed-layer kaolinite-smectite minerals in a red-black soil sequence from basalt in Sardinia (Italy). *Clays Clay Miner.* 52 (4), 473–483.
- Watanabe, T., Funakawa, S., Kosaki, T., 2006. Clay mineralogy and its relationship to soil solution composition in soils from different weathering environments of humid Asia: Japan, Thailand and Indonesia. *Geoderma* 136 (1–2), 51–63.

- Watanabe, T., Hase, E., Funakawa, S., Kosaki, T., 2015. Inhibitory effect of soil micropores and small mesopores on phosphate extraction from soils. *Soil Sci.* 180 (3), 97–106.
- Watanabe, T., Hasenaka, Y., Hartono, A., Sabiham, S., Nakao, A., Funakawa, S., 2017. Parent materials and climate control secondary mineral distributions in soils of Kalimantan, Indonesia. *Soil Sci. Soc. Am. J.* 81 (1), 124–137.
- Ziegler, K., Hsieh, J.C.C., Chadwick, O.A., Kelly, E.F., Hendricks, D.M., Savin, S.M., 2003. Halloysite as a kinetically controlled end product of arid-zone basalt weathering. *Chem. Geol.* 202 (3–4), 461–478.